Anion Association Strength as a Unifying Descriptor for the Reversibility of Divalent Metal Deposition in Non-Aqueous Electrolytes

Justin G. Connell[1,2,*], *Milena Zorko*[1,2,3], *Garvit Agarwal*[1,2], *Mengxi Yang*[1,4], *Chen Liao*[1,4], *Rajeev S. Assary*[1,2], *Dusan Strmcnik*[1,2], *Nenad M. Markovic*[1,2]

[1] *Joint Center for Energy Storage Research, Argonne National Laboratory, Lemont, IL 60439, USA*

[2] *Materials Science Division, Argonne National Laboratory, Lemont, IL 60439, USA*

[3] *Department of Materials Chemistry, National Institute of Chemistry, Hajdrihova 19, Ljubljana SI-1000, Slovenia*

[4] *Chemical Sciences and Engineering Division, Argonne National Laboratory, Lemont, IL 60439, USA*

** Email: jconnell@anl.gov*

Abstract

Developing next generation battery chemistries that move beyond traditional Li-ion systems is critical to enabling transformative advances in electrified transportation and grid-level energy storage. In this work, we provide the first evidence for common descriptors for improved reversibility of metal plating/stripping in non-aqueous electrolytes for multivalent ion batteries. Focusing first on the specific role of chloride (Cl^-) in promoting electrochemical reversibility in multivalent systems, rotating disk (RDE) and ring-disk electrode (RRDE) investigations were performed utilizing a variety of divalent cations (Mg^{2+}, Zn^{2+} and Cu^{2+}) and the bis-(trifluoromethane sulfonyl) imide ($TFSI^-$) anion. By introducing varying concentrations of Cl^-, a cooperative effect is observed between $TFSI^-$ and Cl^- that yields the more reversible behavior of mixed electrolytes relative to electrolytes containing only $TFSI^-$. This effect is shown to be general for Mg, Zn and Cu electrodeposition, and mechanistic understanding of the role of Cl^- in improving reversibility of TFSI-based electrolytes is obtained through the combination of R(R)DE experimental results and density functional theory (DFT) evaluation of the redox activity and thermodynamic stability of various TFSI- and Cl-based solution complexes of metal ions. The cooperative anion effect is further generalized to other mixed anion systems, where systematic variations in anion association strength predicted from DFT (i.e., $Cl^- > OTf^- \sim TFSI^- > BF_4^- > PF_6^-$) yield corresponding trends in redox potentials and improvements of ≥ 200 mV in the reversibility of metal deposition/dissolution. These results identify anion association strength as a common descriptor for the reversibility of divalent metal anodes and suggest a set of general design principles for developing new electrolytes with improved activity and stability.

Keywords

Magnesium, Zinc, Battery, Electrolyte Design, Metal Deposition, Electrochemistry

Table of Contents Figure

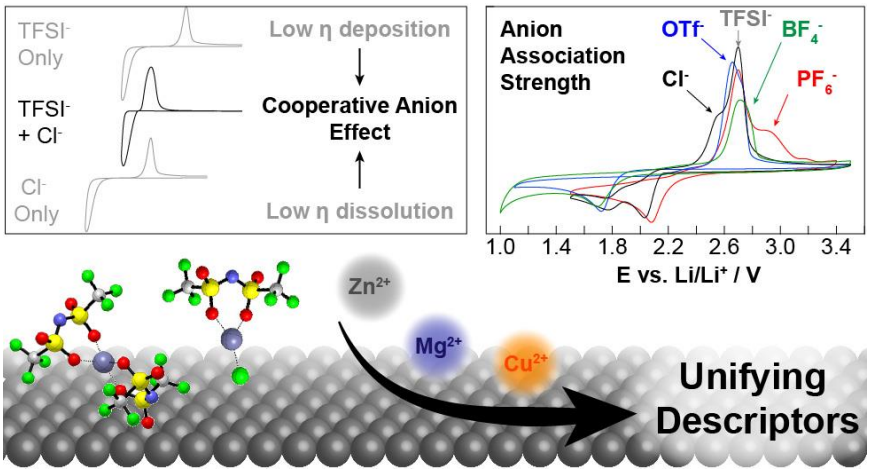

1. Introduction

Developing new battery chemistries that move beyond traditional Li-ion systems is critical to enabling transformative advances such as all-electric transportation and grid-level storage of energy from renewable resources[1]. A particularly promising chemistry for transportation-based battery systems relies on the use of multivalent cations – in particular magnesium (Mg^{2+}) ions – where the implementation of Mg metal as an anode would enable significant gains in both volumetric energy density and total cell cost relative to existing Li-ion systems[2,3]. Following the discovery of the Chevrel-phase cathode for Mg-ion batteries[4], substantial progress has been made in recent years toward developing new, higher-voltage cathodes for Mg-ion batteries[5–12]. Similarly, a variety of different electrolytes for reversible Mg anodes have been developed[13–21], yielding an ever-expanding library of chemistries from which to choose. Despite the wide array of materials and electrolytes available, demonstration of a high voltage multivalent battery that is competitive with existing Li-ion systems remains elusive.

One of the primary challenges facing successful implementation of a high voltage magnesium battery is the fact that many of the most promising electrolytes developed to date are incompatible with either Mg anodes[5,22,23] or, more commonly, high voltage oxide cathodes[24–26], both of which are required in order for such systems to compete with existing Li-ion batteries. One reason for this bottleneck is that many Mg electrolytes rely on the presence of significant concentrations of chloride (Cl^-) to enable reversible metal deposition/dissolution at the anode[27–29], which is incompatible with oxide cathode materials due to parasitic reactions that take place at high voltage (e.g. cathode and current collector corrosion)[26]. Furthermore, understanding of the specific role of Cl^- in improving the reversibility of divalent anodes in nonaqueous electrolytes remains incomplete, with clear evidence only having been provided for Cl^- yielding enhanced protection of the active surface from passivation by oxidizing impurities such as H_2O[28,30]. Broadly speaking, investigations of multivalent anode chemistry are typically focused on a single working cation, making it difficult to identify and understand trends and general design principles for developing new multivalent electrolytes that can enable high voltage full cells.

In this work, we present the first evidence for the existence of common descriptors for deposition/dissolution of metals from divalent cations via a systematic study of multiple combinations of working cations and counter-anions in non-aqueous electrolytes. We first focus on identifying the specific role of Cl^- in promoting reversibility in multivalent systems by using

cyclic voltammetry (CV) along with rotating disk and ring-disk electrode (RDE and RRDE) measurements in the presence of Mg^{2+}, Zn^{2+} and Cu^{2+} with the bis-(trifluoromethane sulfonyl) imide ($TFSI^-$) anion. By introducing varying concentrations of Cl^-, a cooperative effect is observed between $TFSI^-$ and Cl^- that yields the overall more reversible behavior of mixed electrolytes relative to electrolytes containing only $TFSI^-$. This effect is shown to be general for Mg, Zn and Cu electrodeposition, and mechanistic understanding of the role of Cl^- in improving reversibility of TFSI-based electrolytes is provided through the combination of R(R)DE experimental results and density functional theory (DFT) evaluation of the redox activity and thermodynamic stability of various TFSI- and Cl-based solution complexes. The cooperative anion effect is further shown to be general to other dual anion electrolytes with and without Cl^-, where the association strength between constituent anions and the working cation leads to corresponding differences in the onset of metal oxidation and the overall reversibility of metal deposition/dissolution. These trends are again verified by DFT calculations and shown experimentally to be active in both Zn- and Mg-based systems. These results point to the presence of a common descriptor for the activity of divalent metal anodes – anion association strength – and suggest a set of general design principles for developing new electrolytes with improved reversibility and tailorable stability at both anodic and cathodic potentials.

2. Results

2.1 Role of Cl^- in Promoting Reversibility in Mixed TFSI/Cl Electrolytes

We begin by exploring the static voltammetry of Cu-, Zn- and Mg-based electrolytes with only $TFSI^-$, as well as with both $TFSI^-$ and Cl^- present (Figure 1). We will initially focus on the response of "dilute" (0.5-2.0 mM) solutions of the active divalent cations (M^{2+}), as these conditions make it possible to access diffusion-limited behavior and better resolve the relative contributions to the overall electrochemical response of the various electrochemically-active reactants and intermediates that may be present in solution. This is in contrast to "concentrated" electrolyte solutions (e.g., ≥ 0.1 M), where, generally speaking, peaks in the voltammogram are only present due to reversal of the electrochemical sweep during reduction and the dissolution of a fixed quantity of deposited metal on oxidation (Figure S1). Dilute electrolyte conditions also enable rotating (ring) disk electrode (R/RDE) studies to assess diffusion coefficients and reaction kinetics, which will be discussed in detail below. Note that, unless otherwise stated, a supporting electrolyte

of 0.2 M LiTFSI is employed when dilute solutions of the working divalent cation are used in order to provide sufficient electrolyte conductivity to perform electrochemical measurements (see Experimental Methods for additional details). Diglyme is used as solvent in all experiments due to favorable solubility properties for all salts investigated. Finally, we note that glassy carbon is chosen as the working electrode for all experiments in order to avoid surface-specific interactions (e.g., specific adsorption of anions and/or solvent that may take place at metallic surfaces like Au and Pt) and ensure that the intrinsic electrochemistry of the metal deposition process is explored.

Initial examination of the voltammograms in Figure 1 reveal several similarities in the influence of Cl^- on Cu, Zn and Mg electrodeposition. In all cases, the addition of Cl^- to the solution yields an additional oxidation peak, highlighted with downward arrows in Figures 1a-c, which is located at lower potentials (i.e., lower overpotential) relative to the single oxidation peak in TFSI-only electrolytes. In all cases this low overpotential oxidation peak exhibits a lower peak current density than the second oxidation peak. In the case of Zn^{2+} and Mg^{2+}, the addition of Cl^- also results in the presence of an additional reduction peak, highlighted with upward arrows in Figure 1b-c. We note that slower scan rates were used for all Zn experiments relative to Mg and Cu (10 mV s^{-1} vs. 50 mV s^{-1}) due to overlap of these two reduction features at higher scan rates (Figure S2). The second reduction wave for Mg is obscured by a significant amount of parasitic reduction current, which is the result of simultaneous decomposition of $TFSI^-$ at cathodic potentials that is also observed in voltammetry of the Mg^{2+}-free supporting electrolyte (Figure S3). This parasitic current also necessitated the higher Mg^{2+} concentrations used in this work relative to Zn^{2+} and Cu^{2+} (see Experimental Methods for additional details). For both Mg^{2+} and Zn^{2+}, the additional oxidation peak disappears when the lower potential vertex is restricted such that the second reduction wave is not accessed (Figure S4), indicating that these redox features are related. The presence of an additional reduction wave is particularly surprising, as only a single, 2 e^- reduction mechanism is expected for electrodeposition in these systems[31], although we note that the lowest potentials accessed in Ref. 31 are positive of those where the onset of the second plateau is observed in this work. This is in contrast to Cu^{2+} electrochemistry, where an additional reversible couple is observed at ca. 3.7 V that corresponds to the 1 e^- reduction of Cu^{2+} to Cu^+ [32]. The addition of Cl^- further improves the reversibility of this process, consistent with observations in aqueous media[33,34]. In order to better understand the role of Cl^- in modifying the electrochemical response, we will first focus on the electrochemistry of Zn^{2+} in the subsequent R(R)DE analysis.

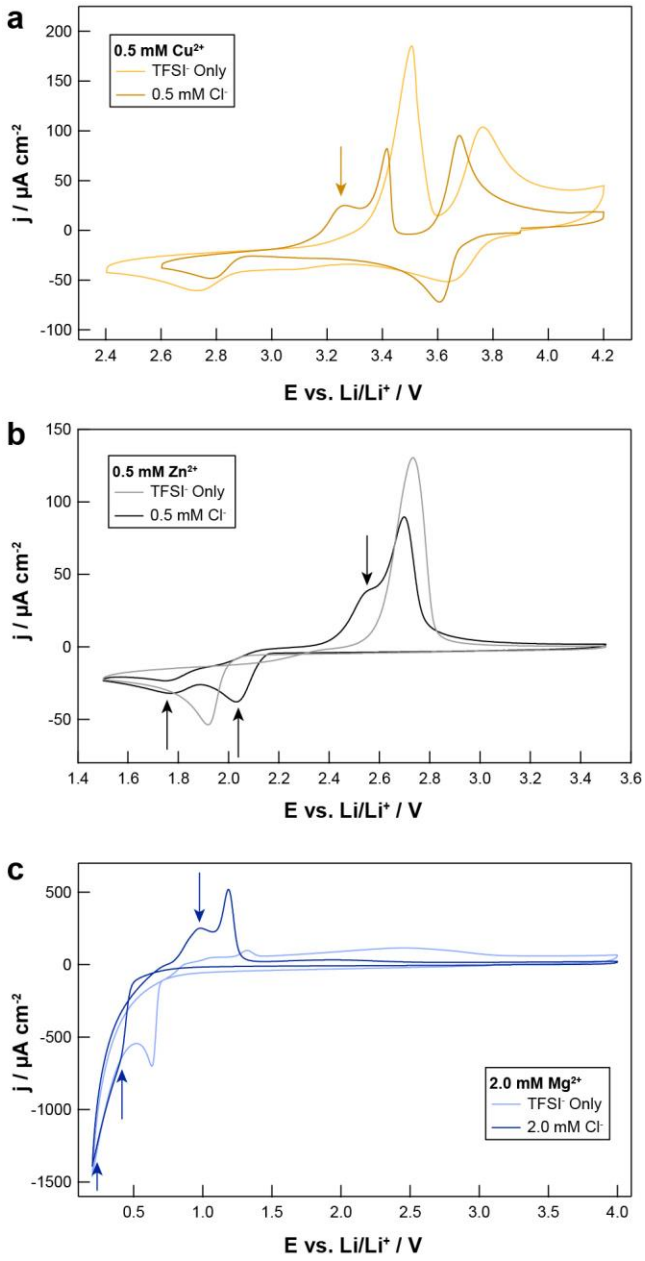

Figure 1. CVs of electrolytes with (a) 0.5 mM Cu^{2+} (b) 0.5 mM Zn^{2+} and (c) 2.0 mM Mg^{2+} added with and without an equal concentration of Cl^- present. Arrows highlight the additional redox peaks observed upon the addition of Cl^-. Scan rates are 50 mV s^{-1} for Cu^{2+} and Mg^{2+} electrolytes, and 10 mV s^{-1} for Zn^{2+} electrolytes.

Consistent with the static CV measurements, RDE voltammetry of 0.5 mM Zn^{2+} electrolytes with 0.5 mM Cl^- yields two diffusion-limited reduction plateaus (Figure 2a) whose onsets match those of the two reduction waves present in static measurements. Both reduction plateaus exhibit Levich-type behavior as a function of rotation rate (Figure 2b) with thermodynamic potentials (as measured on the reverse scan) of 2.30 and 1.95 V. Furthermore, both

plateaus exhibit hysteresis; i.e., more negative potentials are needed to initiate reduction on the forward scan relative to the potentials at which reduction ceases on the reverse sweep. This suggests that both reduction waves are related to metal deposition, as this hysteresis is consistent with the presence of a nucleation overpotential for both plateaus. In order to confirm the origin of these reduction waves, rotating ring-disk electrode (RRDE) voltammetry was employed. By holding the ring electrode at a negative potential in order to drive constant Zn deposition, perturbations to the steady-state Zn deposition current on the ring during potential sweeps on the disk indicate changes to the concentration of Zn^{2+} available for electrodeposition. Holding the ring at 2.1 V vs. Li/Li^+ (corresponding to the first reduction plateau, Figure 2c) results in current response on the ring that mirrors that at the disk, with the increase in reduction current on the disk from both the first and second reduction plateaus yielding a corresponding decrease in the steady-state reduction current at the ring. Similar experiments with the ring held at 1.5 V vs. Li/Li^+ yield the same response (Figure S5a). Additional RRDE measurements performed with the ring held at an anodic potential of 3.5 V yield no significant oxidation current as the potential of the disk is swept (Figure S5b), clearly demonstrating that the presence of two reduction plateaus is not related to sequential 1 e^- transfer steps, e.g. via the formation of Zn^+. This stands in contrast to RRDE measured for $Cu^{2+/+}$ redox with E_{ring} = 3.90 V (Figure S5c), which clearly shows ring current related to the re-oxidation of Cu^+ to Cu^{2+} and further supports the observation that no single electron redox takes place for Zn^{2+}. As a result, we conclude that the consumption of Zn^{2+} at the disk electrode by both reduction waves is the result of Zn metal deposition.

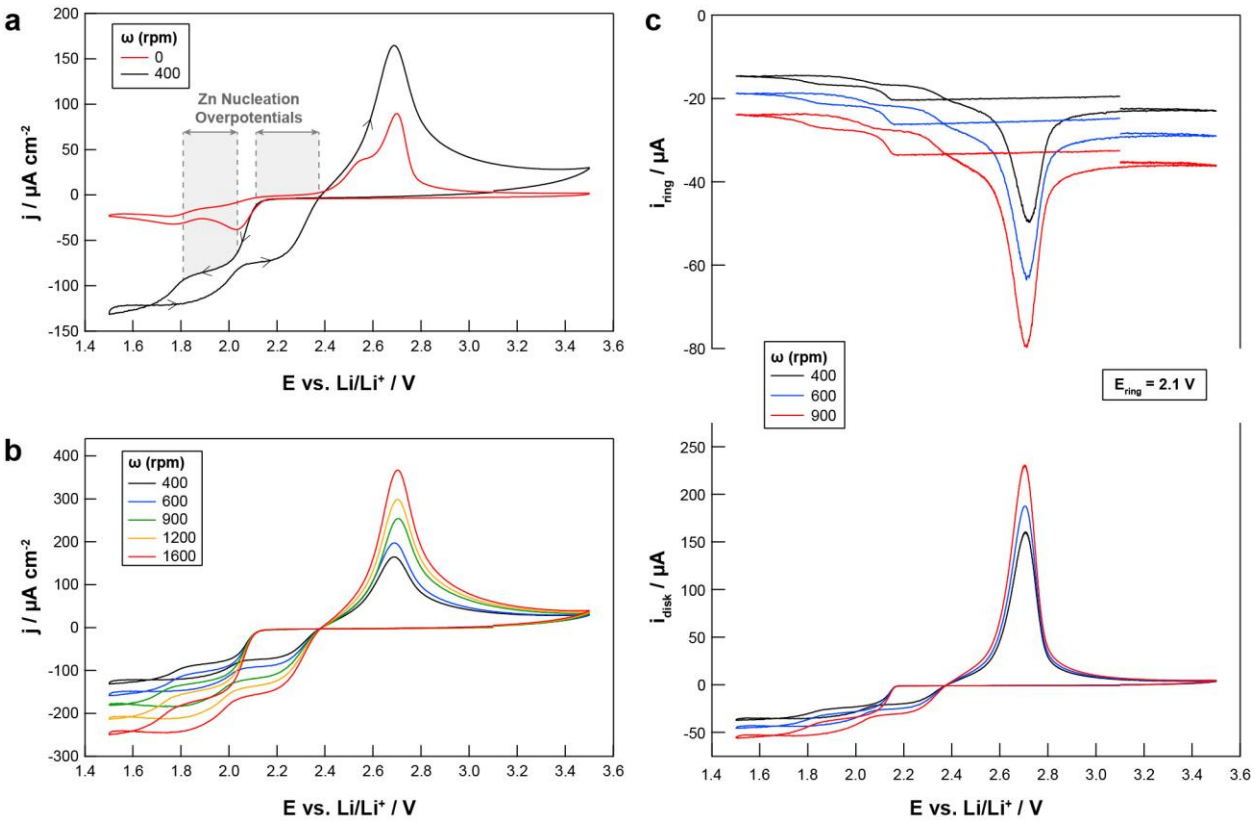

Figure 2. (a) Comparison of CV response with no rotation (red) and rotation at 400 rpm (black). The presence of nucleation overpotentials is denoted by the gray boxes. (b) RDE measurements as a function of rotation rate. (c) RRDE measurements showing evolution of the ring current under potentiostatic conditions (E_{ring} = 2.1 V, top) as the disk potential is swept (bottom) with different rotation rates. All electrolytes contain 0.5 mM Zn^{2+} and 0.5 mM Cl^-. Scan rate for all CVs is 10 mV s^{-1}.

2.2 Effect of Cl^- Concentration on Zn^{2+} Speciation

Having confirmed that both reduction waves are related to Zn deposition, the question arises as to why two separate reduction events are present in the first place, as only a single, 2 e^- transfer process is expected for Zn metal deposition. In order to better understand the origins of this effect, RDE measurements were performed in the presence of varying concentrations of Cl^- (Figure 3a). In this analysis we focus on the reverse scan to assess the potentials at which metal deposition ceases, which corresponds to the thermodynamic potential for metal plating. In doing so we also avoid analyzing metastable regions where nucleation overpotentials are present, as these can change in response to differences in extrinsic factors such as electrode roughness, cleanliness and history (e.g. cycling). Consistent with static CV measurements that exhibit a single reduction peak (gray curve, Figure 1b), Cl-free electrolytes exhibit only one diffusion-limited plateau between 1.5 and 2.2 V. Notably, the magnitude of the diffusion-limited current density for Cl-free

electrolytes is approximately 40% higher than the maximum observed for any of the Cl-containing electrolytes (e.g., 0.32 vs. 0.24 mA cm^{-2} for Cl-free vs. 0.67 mM Cl^- at 1600 rpm). Koutecky-Levich analysis[35] of all electrolytes at 1.8 V (Figure 3b) reveals this difference in limiting current density stems from differences in the diffusion coefficient (D_0) of the active solution species. The Cl-free electrolyte yields a value of $D_0 = 2.9 \times 10^{-5}$ cm^2 s^{-1}, whereas electrolytes with Cl^- present exhibit more or less identical diffusion coefficients of $1.9 \pm 0.1 \times 10^{-5}$ cm^2 s^{-1}. The apparently slower diffusion of Zn^{2+} upon the addition of Cl^- to TFSI-containing electrolytes suggests that anion chemistry influences the diffusivity of Zn^{2+}, a finding that will be explored further below.

Focusing on the Cl-containing electrolytes, two noteworthy changes take place as the Cl^- content is increased. First, the magnitude of the diffusion-limited current density of the first reduction plateau decreases as the Cl^- content is increased. Second, there is an increase in the amount of oxidation current present at lower overpotential, with an additional peak resolved at ca. 2.5 V for the highest Cl^- content measured (0.67 mM). This clear dependence of the RDE response with Cl^- concentration strongly suggests that the two redox peaks observed in mixed $TFSI^-/Cl^-$ electrolytes are the result of metal deposition/dissolution from two separate solution complexes. The first reduction wave likely derives from a TFSI-only (or at least TFSI-rich) Zn^{2+} complex, given that its relative contribution to the overall deposition current decreases as the Cl^- content increases. Furthermore, the thermodynamic potential of this reduction wave is identical to that observed for Cl-free electrolytes. It then follows that the second plateau likely corresponds to Zn deposition from a Cl-rich solution complex. Unlike the first reduction feature, which varies in response to the concentration of the TFSI-rich solution complex, the magnitude of the current density of the second plateau is identical for all three Cl^- concentrations due to the identical total Zn^{2+} concentration. In other words, the contribution of the Cl-rich solution species to the total Zn plating current increases relative to the TFSI-rich species; however, the maximum limiting current density is fixed by the total Zn^{2+} concentration available for plating. Again utilizing Koutecky-Levich analysis (Figure 3c), it is possible to estimate the approximate concentration of the TFSI-rich Zn complex (assuming that the diffusivity of this species is the same as that measured in TFSI-only electrolytes), revealing its concentration decreases from 0.38 mM to 0.25 to 0.17 mM in the presence of 0.33, 0.50 and 0.67 mM Cl^-, respectively.

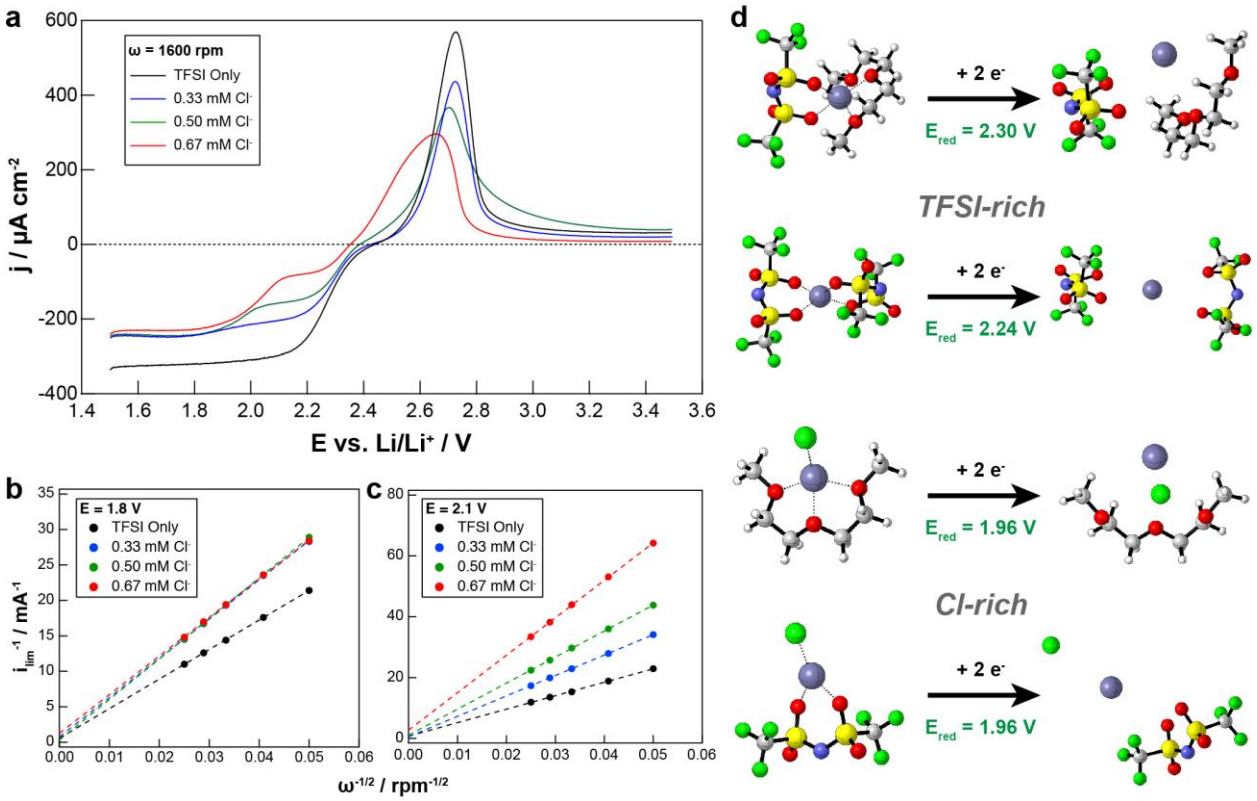

Figure 3. (a) RDE voltammetry measured at ω = 1600 rpm demonstrating the effect of Cl^- addition on Zn deposition/dissolution. The total Zn^{2+} concentration is 0.5 mM for all Cl^- concentrations. (b-c) Koutecky-Levich analysis as a function of Cl^- concentration for Zn plating at (b) E = 1.8 V and (c) E = 2.1 V. (d) DFT calculations of 2 e^- reduction potentials of stable Zn^{2+} solution complexes and the optimized structures before and after 2 e^- reduction. From top to bottom: 1 diglyme + 1 $TFSI^-$, 2 $TFSI^-$, 1 Cl^- + 1 diglyme, 1 Cl^- + 1 $TFSI^-$.

To gain insight into whether the presence of multiple Zn^{2+} solution complexes is reasonable, density functional theory (DFT) calculations were performed to investigate the thermodynamic stability and expected reduction potential of Zn^{2+} complexes with multiple combinations of Cl^-, $TFSI^-$ and diglyme. A summary of 1 e^- and 2 e^- reduction potentials for all species investigated with DFT is given in Table S1. Several of the combinations simulated were found to be unstable to single electron transfer (i.e., exhibited breaking of chemical bonds upon electron attachment), and in some cases were unstable to direct two-electron transfer as well. Of the complexes that were found to be stable, many would spontaneously reduce (i.e., were calculated to have reduction potentials ≥ 2.4 V, which is the highest potential at which any Zn^{2+} reduction is observed experimentally) or would be electrochemically inactive under our experimental conditions (i.e., have reduction potentials ≤ 1.5 V, which is the lowest potential accessed in this work for Zn). With these criteria in mind, four solution species were identified as

stable to both one and two electron reduction with reasonable thermodynamic potentials and are summarized in Figure 3d. The DFT-predicted reduction potentials for these complexes are consistent with the thermodynamic potentials of the two reduction plateaus measured with RDE. Specifically, Zn^{2+} coordinated with one $TFSI^-$ anion and either one diglyme or a second $TFSI^-$ yields predicted reduction potentials of 2.30 and 2.24 V vs. Li/Li^+, respectively, as compared with 2.30 V observed experimentally for the first reduction wave. Furthermore, Zn^{2+} coordinated by one Cl^- and either one $TFSI^-$ or one diglyme yields a predicted reduction potential of 1.96 V, as compared with 1.95 V observed experimentally for the second reduction wave. Not only do the DFT calculations reproduce the experimentally observed reduction potentials, but the specific solution species also match the hypothesis that the first plateau derives from a TFSI-rich Zn coordination, while the second plateau derives from a Cl-rich coordination. We hypothesize that it is more likely that the speciation of the "Cl-rich" coordination is closer to the mixed TFSI/Cl structure than the diglyme/Cl structure, as experiments below with other mixed anion systems strongly suggest the presence of mixed anion coordination rather than significant participation of diglyme. We also note that this close agreement between experiment and theory is further supported by separate calculations of anion reduction potentials (Table S2), which also predict the onset of $TFSI^-$ reduction (E_{DFT} = 0.93 V) measured in divalent cation-free supporting electrolyte (E_{exp} = 0.91 V, Figure S3).

2.3 Cooperative Anion Effect and the Role of Anion Association Strength

Regardless of the specific identity of the solution complexes leading to the two reduction waves for Zn plating, a novel effect can be proposed from the RDE data in Figure 3a, with general implications for the role of Cl^- in improving reversibility. What is clearly shown is that as the Cl^- concentration increases, a larger fraction of Zn dissolution takes place at lower overpotential. Simultaneously, a larger fraction of the diffusion-limited current for Zn deposition can only be accessed at higher overpotentials. These observations suggest that while Cl^- appears to lower the overpotential required to dissolve Zn metal, it also increases the overpotential required to drive metal deposition. Conversely, these data also suggest that while $TFSI^-$ yields a low overpotential for metal deposition (consistent with the identical onset potentials for the first plateau in mixed electrolytes and the only plateau observed for TFSI-only electrolytes), it also results in a high

overpotential for metal dissolution. Taken together, this behavior suggests a cooperative effect between $TFSI^-$ and Cl^- that leads to the overall more reversible behavior in this system.

This cooperative anion effect can be rationalized in terms of the relative association strength between the constituent anions and the divalent cation, with Cl^- binding to Zn^{2+} considerably more strongly than $TFSI^-$. The magnitude of these differences was determined via DFT calculations of anion-cation binding energies (Tables S3 and S4), and indicates that, depending on the speciation, the interaction between Zn^{2+} and Cl^- is 0.8-2.3 eV stronger than that between Zn^{2+} and $TFSI^-$. Differences in anion association strength are further consistent with the lower value of D_0 measured in Cl-containing electrolytes, with the more tightly bound Cl-containing complexes restricting the mobility of Zn^{2+} relative to Zn^{2+} coordinated with $TFSI^-$ only. Note that as the current from the second plateau is the sum of contributions from both active species and the concentration of this second species is unknown, the value of D_0 calculated above only represents an upper limit and is likely lower.

The consequence of the apparent difference in anion association strength can be summarized in terms of its effect on the deposition and dissolution half-reactions. For the deposition half-reaction (ignoring for the moment the contribution of nucleation overpotential and surface-specific effects), there is a lower energy penalty required to desolvate Zn^{2+} from a coordination environment that is TFSI-rich due to the weaker association strength as compared with Cl^-. As a result, metal deposition is observed to initiate at lower overpotential from Zn^{2+} in a TFSI-rich coordination (i.e., plateau 1) relative to Zn^{2+} in a Cl-rich coordination (i.e., plateau 2). During metal dissolution, this relationship is reversed. Because Cl^- binds more strongly to Zn^{2+}, there is a higher driving force to re-solvate Zn^{2+} species into a Cl-rich coordination environment as compared to a more weakly-associating, TFSI-rich coordination. As a result, Zn dissolution is observed to initiate at a lower overpotential in the presence of Cl^-, with the relative amount of low overpotential dissolution increasing with increasing Cl^- concentration. We note that the individual contributions of $TFSI^-$ and Cl^- are able to be resolved at dilute concentrations; however, the effect at high concentrations is simply a more reversible reaction, with single peaks present at the lowest accessible overpotentials for the deposition and dissolution half-reactions since both anions are present in significant excess (Figure S1).

2.4 Observation of Cooperative Anion Effect for Multiple Divalent Cations

Although results up to this point have focused on Zn^{2+} specifically, the cooperative anion effect detailed above has general implications for the electrodeposition of divalent metals in non-aqueous media. In particular, as the overpotentials for the deposition and dissolution half-reactions in dual anion electrolytes would, to first order, be guided by the association strength between the constituent anions and the active cation, this effect should be observable regardless of the specific divalent cation. Equally significantly, this effect should be tailorable depending on the specific anions chosen for the electrolyte. We will focus first on extending this concept to other divalent cations, as evidence for this has already been presented in Figure 1. As shown in these data, the addition of Cl^- to Zn^{2+}, Mg^{2+} and Cu^{2+} electrolytes containing $TFSI^-$ results in nearly identical behavior: the appearance of a second oxidation wave to lower overpotential relative to the main oxidation peak and, in the case of Zn^{2+} and Mg^{2+}, the presence of an additional reduction wave to higher overpotential.

Although there does not appear to be an obvious second reduction feature for Cu^{2+}, this difference is likely due at least in part to the presence of the reversible $Cu^{2+/+}$ couple that is not observed for Zn^{2+} or Mg^{2+}. Nevertheless, changes in the electrochemical response are consistent with the cooperative anion effect proposed in this work. In the absence of significantly different overpotentials for the different deposition species, one would expect that the reversible potential for metal deposition would move to lower potentials (i.e., higher overpotential) as the concentration of Cl^- increases. This is because the increasing fraction of Cl^- ions coordinating the working cation should still increase the desolvation penalty required to initiate the deposition half-reaction. Indeed, RDE measurements of Cu^{2+} electrolytes with varying Cl^- content (Figure S6) reveal that the thermodynamic potential for metal deposition shifts to consistently more negative potentials as the Cl^- concentration increases (as much as 100 mV more negative for 0.67 mM Cl^- relative to Cl-free electrolytes). Also analogous to Zn-containing electrolytes, the diffusivity of Cu^+ decreases in the presence of Cl^- (D_0 = 1.7 x 10^{-5} and 3.2 x 10^{-6} cm^2 s^{-1} for 0.00 and 0.67 mM Cl^-, respectively). Due to the proximity of Mg electrochemistry to Li electrodeposition potentials in the LiTFSI supporting electrolyte, it was only possible to access diffusion-limited conditions in Cl-free Mg electrolytes (Figure S7); however, a similar negative shift of the crossover potential is observed in static CVs comparing Cl-free and Cl-containing electrolytes (0.72 vs. 0.64 V, respectively, Figure 1c). DFT calculations of an identical set of $TFSI^-$/Cl^-/diglyme coordination

environments to those performed for Zn^{2+} (Table S1) reveal a larger number of unstable Mg^{2+} complexes. In all cases this instability is driven by dissociation of the S-CF_3 bond in $TFSI^-$ upon 1 and/or 2 e^- reduction. This breakdown mechanism is consistent with experimental observations of intrinsic $TFSI^-$ reduction at the potentials required for Mg electrodeposition (Figure S3), as well as with previous studies suggesting instability of the $TFSI^-$ anion during Mg^{2+} reduction[36–38]. Nevertheless, some complexes of Mg with $TFSI^-$ are predicted to be stable, in particular Mg^{2+} coordinated by one diglyme and one $TFSI^-$, which exhibits a predicted reduction potential of 0.75 V that matches the thermodynamic potential measured from RDE quite well (E_{exp} = 0.85 V). Taken together, these results provide significant evidence that the cooperative anion effect is active regardless of the nature of the divalent cation and may therefore serve as a general design principle for developing more reversible electrolytes.

2.5 Anion Association Strength as a Unifying Descriptor

As the central hypothesis underlying the cooperative anion effect is that overpotentials for the deposition and dissolution half reactions are guided by differences in association strength between the constituent anions and the working cation, it follows that this effect must be active beyond mixtures of $TFSI^-$ and Cl^-. Indeed, voltammetry utilizing mixtures of the chemically similar trifluoromethanesulfonate (triflate, OTf^-) anion with Cl^- (with 0.2 M LiOTf as the supporting electrolyte, in analogy to the $TFSI^-$ studies above) yield very similar response to that of $TFSI^-/Cl^-$ mixtures for both Zn^{2+} and Mg^{2+} (Figures S8 and S9). For both Zn^{2+} and Mg^{2+}, two reduction features are again observable, suggesting that multiple solution species are also active in these systems. In contrast to $TFSI^-/Cl^-$ mixtures, however, there is only one apparent oxidation wave for Zn dissolution at 2.48 V. This suggests that the overpotential for Zn dissolution into an OTf-rich complex is closer to that of Cl^- than in the case of $TFSI^-$ and results in overlapping oxidation peaks. The DFT calculations support this hypothesis, where Zn^{2+}-diglyme complexes exhibit similar or stronger association strengths with two OTf^- (ΔG = -0.99 eV) compared to two $TFSI^-$ anions (ΔG = -0.91 eV), as well as similar or lower computed reduction potentials (Tables S3 and S4). Previous work comparing the bulk speciation of Zn electrolytes with $TFSI^-$ and OTf^- has also shown evidence of stronger association of Zn with OTf^- relative to $TFSI^-$, consistent with our experimental observations[39].

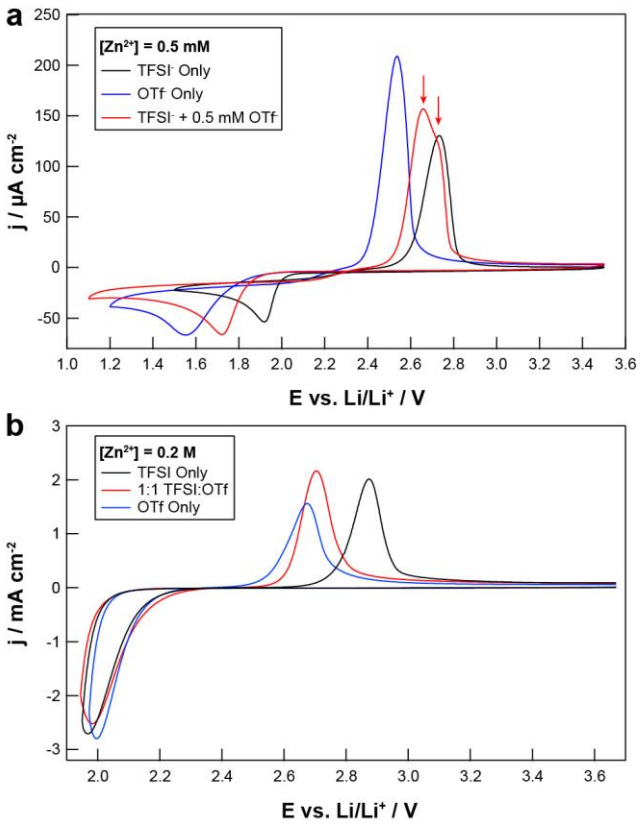

Figure 4. (a) CVs of 0.5 mM Zn^{2+} electrolytes with $TFSI^-$ only, OTf^- only, and TFSI + 0.5 mM OTf^- added. Supporting electrolyte is 0.2 M LiTFSI for TFSI-only and $TFSI^-$ + 0.5 mM OTf^- voltammetry, and 0.2 M LiOTf for OTf-only voltammetry. Arrows indicate the position of the two oxidation peaks in the mixed TFSI/OTf electrolyte. Scan rate is 10 mV s^{-1}. (b) CVs of 0.2 M Zn^{2+} electrolytes exhibiting the same response as the corresponding dilute electrolytes. Total charge passed on deposition is 2.5 ± 0.2 mC for all CVs. Scan rate is 50 mV s^{-1}.

If the OTf^- anion can indeed lower the dissolution overpotential for Zn, it follows that a mixture of OTf^- with $TFSI^-$ should exhibit similar behavior to that of $TFSI^-$ with Cl^- (i.e., an additional oxidation wave at lower overpotential relative to that deriving from $TFSI^-$). CV measured in mixed $TFSI^-/OTf^-$ electrolytes with Zn^{2+} present yield this exact behavior (red curve, Figure 4a), with two clearly distinguishable oxidation waves. Comparing this behavior with voltammetry in TFSI- and OTf-only electrolytes (black and blue curves, respectively, Figure 4a) reveal the higher overpotential oxidation peak overlaps exactly with that deriving from TFSI-only electrochemistry, whereas the lower overpotential oxidation peak exhibits a value intermediate to that of TFSI-only and OTf-only voltammetry, suggesting Zn^{2+} solvation by a mixed $TFSI^-/OTf^-$ coordination environment. In contrast to $TFSI^-/Cl^-$ mixtures, $TFSI^-/OTf^-$ electrolytes exhibit only one reduction peak on deposition, suggesting that mixed coordination drives electrodeposition in

this system, similar to Cu^{2+} above (Figure 1a). Consistent with this explanation, the deposition peak for $TFSI^-/OTf^-$ electrolytes is exactly intermediate to that of the TFSI- and OTf-only electrolytes.

Having demonstrated the cooperative anion effect is active for mixtures of $TFSI^-$ with anions of greater association strength (i.e., Cl^- and OTf^-), the question arises as to whether more weakly associating anions can also yield changes in deposition/dissolution overpotentials. In order to test this hypothesis, similar mixed anion electrolytes were explored utilizing BF_4^- and PF_6^-, both of which are predicted by DFT (Table S4) to form Zn^{2+}-diglyme and Mg^{2+}-diglyme complexes with weaker association strengths than those with $TFSI^-$ (e.g., for 2 BF_4^- anions ΔG = -0.33 eV and -0.72 eV, and with 2 PF_6^- anions ΔG = +0.11 eV and -0.23 eV for Zn^{2+} and Mg^{2+}, respectively). The voltammetry of all anion mixtures with $TFSI^-$ explored in this work are summarized in Figure 5a and reveal a striking trend. CV in all electrolytes exhibit one oxidation peak at the same potential (2.7 V vs. Li/Li^+), corresponding to metal dissolution and Zn^{2+} solvation by $TFSI^-$. As the anion association strength is systematically increased (i.e., $Cl^- > OTf^- \sim TFSI^- > BF_4^- > PF_6^-$), the position of the second oxidation peak shifts from below that of $TFSI^-$ (Cl^- and OTf^-) to above that of $TFSI^-$ (BF_4^- and PF_6^-), in precise agreement with the trends in reduction potentials predicted by DFT (Figure 5b). Furthermore, the plating half reaction in $TFSI^-/PF_6^-$ electrolytes is shifted to higher potentials (i.e., lower overpotential) relative to all other electrolytes. This is consistent with the expectation that a more weakly-associating anion than $TFSI^-$ should result in a lower deposition overpotential than is accessible in electrolytes where $TFSI^-$ is the most weakly-coordinating species. We note that these results suggest that solvation structure changes significantly as the cation approaches the electrified interface. This is because anions such as $TFSI^-$ and PF_6^-, which are nominally weakly-coordinating in the electrolyte bulk[18,39–41], clearly play a significant role in guiding deposition/dissolution and therefore must more closely associate with the cation near the electrode surface.

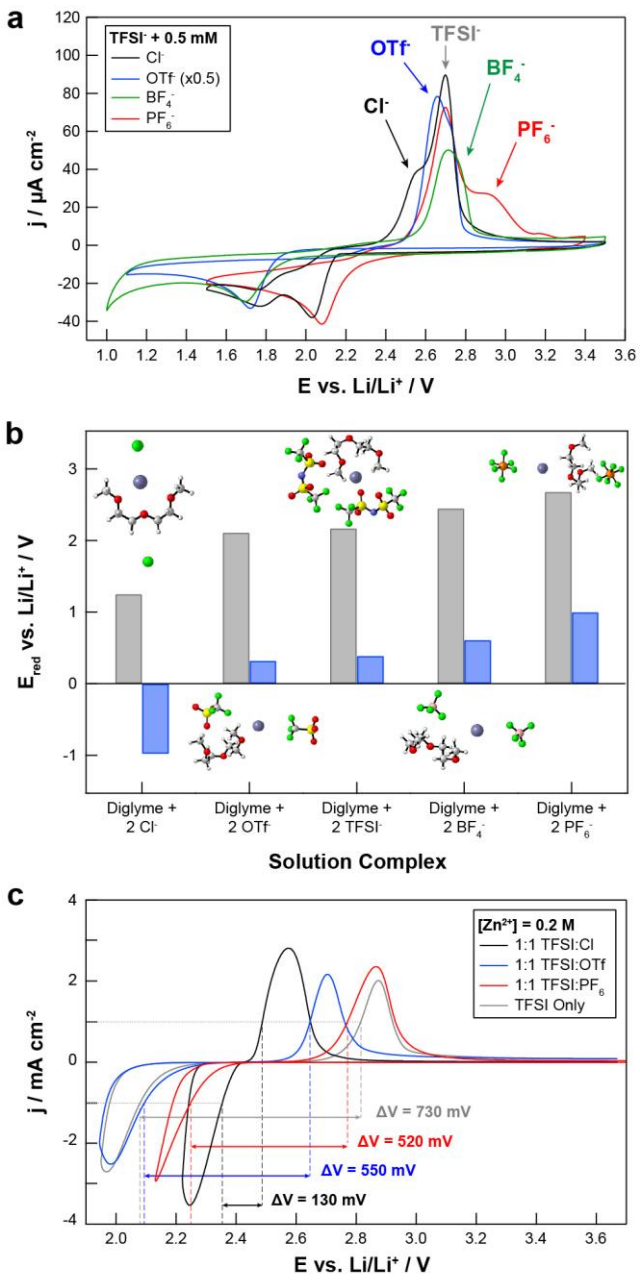

Figure 5. (a) CVs of 0.5 mM Zn^{2+} solutions with $TFSI^-$ and 0.5 mM Cl^-, OTf^-, BF_4^- and PF_6^-. Scan rate is 10 mV s^{-1}. (b) Summary of DFT calculations of 2 e^- reduction potentials for Zn^{2+} (gray) and Mg^{2+} (blue) complexed by one diglyme and two anions. The corresponding optimized reduced Zn^{2+} structures are shown as well. (c) CVs of 0.2 M Zn^{2+} solutions with a 1:1 ratio of $TFSI^-$ with Cl^-, OTf^- and PF_6^-. A TFSI-only CV is shown as well for comparison. 1:1 TFSI:PF_6 electrolyte is a mixture of 0.2 M $ZnTFSI_2$ and 0.4 M $LiPF_6$, all others contain only Zn^{2+}. Total charge passed on deposition is 2.6 ± 0.2 mC for all CVs. Scan rate is 50 mV s^{-1}.

To this point we have focused exclusively on "dilute" electrodeposition response, but for the cooperative anion effect to be truly meaningful for designing new electrolytes, these effects

must also extend to electrolytes with concentrations relevant to battery systems. To investigate whether this is indeed the case, CVs were first measured for concentrated electrolytes with only $TFSI^-$, only OTf^- and a 1:1 $TFSI^-$:OTf^- mixture (0.2 M total Zn^{2+} content, Figure 4b). In direct analogy to the dilute data, the 1:1 $TFSI^-$:OTf^- mixture exhibits an oxidation peak at intermediate potentials to those of the TFSI- and OTf-only electrolytes. Note that these comparisons were performed with a fixed charge passed on deposition in order to ensure that the same amount of metal is dissolved on oxidation in all cases. Concentrated 1:1 mixtures of $TFSI^-$ with Cl^-, OTf^- and PF_6^- all reveal lower overpotentials (measured at deposition/dissolution current densities of 1.0 mA cm^{-2}) as compared with TFSI-only electrolytes (Figure 5c) demonstrating that the addition of a second anion with higher or lower association strength yields significant improvements in reversibility ($\geq$ 200 mV). Note that a mixture of $LiPF_6$ with $ZnTFSI_2$ was used to generate the 1:1 TFSI:PF_6 electrolyte (red curve, Figure 5c) due to issues with impurities present in the custom-synthesized $Zn(PF_6)_2$ salt (see Supporting Information for additional details). These electrolytes also exhibit a shift of the onset of reduction to lower overpotential, consistent with behavior of the dilute TFSI/PF_6 electrolytes. These data indicate that trends observed in dilute voltammetry are active in more concentrated electrolytes, and further support the hypothesis that anion association strength can serve as a descriptor for reversibility in mixed anion electrolytes. Overall, these results point to the broad design space that is available to tailor the reversibility and stability of mixed anion electrolytes for multivalent batteries.

3. Conclusions

In this work, systematic analysis of the impact of anion chemistry on the electrochemical response of divalent electrolytes reveal the presence of a previously unknown cooperative anion effect. This effect is shown to explain the improvements in reversibility observed upon the addition of Cl^- to TFSI-containing electrolytes with Mg^{2+}, Zn^{2+} and Cu^{2+} present as the working cation. Specifically, the more strongly-coordinating Cl^- anion lowers the overpotential for the metal dissolution half-reaction due to the higher driving force for re-solvating divalent cations into a Cl-rich coordination environment, whereas the more weakly-coordinating $TFSI^-$ anion lowers the overpotential for metal deposition half-reaction due to the lower energy penalty to desolvate divalent cations from a TFSI-rich coordination environment. The lowering of both overpotentials for the constituent half-reactions results in an overall more reversible electrochemical couple. In

addition to demonstrating that this effect is active for multiple working cations, the cooperative anion effect is further shown to be general to other mixed anion systems, where the relative association strengths between the constituent anions and the working cation systematically modify the overpotentials for metal deposition/dissolution, resulting in more reversible electrochemical response than is achievable in the TFSI-only electrolyte. These results point to a new set of general design rules for developing more reversible electrolytes that avoid the use of Cl^-, enabling compatibility with high voltage oxide cathodes. We emphasize that the anions chosen in this work are by no means optimized, but are instead constrained by those that are available commercially, or in the case of $Zn(BF_4)_2$ and $Zn(PF_6)_2$, were thankfully able to be synthesized by collaborators. In particular, challenges with removing impurities from $Zn(PF_6)_2$ electrolytes highlight the challenges associated with designing new salts for multivalent batteries. Nevertheless, through the application of computational screening and chemical intuition it will almost certainly be possible to identify other combinations of anions that would exhibit even better performance than those investigated here, and we believe that exploration of this design space represents a new frontier in the field of battery electrolyte development.

4. Experimental Methods

Zinc Salt Synthesis: Zinc carbonate (basic), tetrafluoroboric acid (48 wt% in H_2O), silver hexafluorophosphate (98%) were purchased from Sigma-Aldrich, and zinc bromide (anhydrous) was purchased from Millipore-Sigma. The solvents were purchased as anhydrous grade from Sigma-Aldrich and were stored in an argon-filled glovebox before use.

$Zn(BF_4)_2$ was prepared according to a reported procedure[39]. The salt was recrystallized by diffusing diethyl ether to an acetonitrile solution and was dried overnight at 80 °C under vacuum in an argon-filled glovebox before use.

$Zn(PF_6)_2$ was prepared by a modification of the reported procedure.[1] In an argon-filled glovebox, $ZnBr_2$ (400 mg, 1.78 mmol) was suspended in ~20 mL of anhydrous acetonitrile, to which $AgPF_6$ (880 mg, 3.5 mmol) was slowly added. The solution was allowed to stir in the dark overnight, and then the yellow-green precipitate was removed by filtering through Celite. A copious amount of diethyl ether was added to the filtrate, and a white solid precipitated from the solution. The solid was collected by filtration and washed with two portions (~ 5mL each) of pentane to afford $Zn(PF_6)_2$ as a white powder (380 mg, 60% yield). The salt was dried at room temperature under vacuum in an argon-filled glovebox overnight before use.

Electrolyte Synthesis: $Mg(TFSI)_2$, $Zn(TFSI)_2$, $Cu(TFSI)_2$, NaTFSI (99.5%, Solvionic); $CuCl_2$, $ZnCl_2$ (anhydrous, ≥99.995% trace metals basis, Sigma Aldrich); $Zn(OTf)_2$ (98%, Sigma Aldrich); $MgCl_2$ (Beantown Chemical, 99.99% trace metals basis); $Mg(OTf)_2$ (98%, Alfa Aesar); LiTFSI (Purolyte®, Novolyte Technologies); Tetrabutylammonium

TFSI (≥99%, Sigma Aldrich); $LiPF_6$ (Purolyte®, Novolyte Technologies); and LiOTf (99.995% trace metals basis, Sigma Aldrich) were all dried under vacuum at temperatures ≥100ºC for ≥48 hours prior to use. $Zn(PF_6)_2$ and $Zn(BF_4)_2$ were synthesized as described above and used without further drying. Diglyme (≥99% spectrophotometric grade, Sigma Aldrich) was dried under activated basic alumina for ≥ 48 hours and then distilled under vacuum over Na/K alloy, yielding H_2O content <0.2 ppm as measured by Karl Fischer titration.

For all experiments, 0.2 M solutions of Mg^{2+} and Zn^{2+}, and 0.1 M Cu^{2+} (lower concentration due to solubility issues) were first mixed and allowed to stir overnight before use. In the case of "concentrated" CV measurements, these solutions were used without additional preparation. For "dilute" measurements, a 0.2 M solution of LiTFSI was first mixed and added to the electrochemical cell. After cell assembly, an aliquot of the "concentrated" divalent cation solution was then added to achieve the desired working cation concentration. For example, 12.5 µL of 0.2 M $ZnTFSI_2$ was added to 5.0 mL of the 0.2 M LiTFSI working electrolyte and stirred to yield a final concentration of 0.5 mM Zn^{2+}. Note that a higher concentration of Mg^{2+} relative to Cu^{2+} and Zn^{2+} was required in order to observe Mg plating/stripping currents due to the significant $TFSI^-$ reduction current also present in this potential region. We also note that 2.0 mM Mg^{2+} corresponds to 48 parts-per-million (ppm), whereas 0.5 mM Zn^{2+} and Cu^{2+} corresponds to ~ 33 ppm, indicating that from a mass perspective, these concentrations are actually similar. Mixed anion solutions were made in a similar way, utilizing concentrated electrolytes with varying TFSI:anion ratios but constant total Zn^{2+} concentration (e.g., 1:1 TFSI:Cl from a 0.1 M $ZnTFSI_2$ + 0.1 M $ZnCl_2$ solution, 2:1 TFSI:Cl from 1.33 M $ZnTFSI_2$ + 0.067 M $ZnCl_2$, etc…). As dilute electrolytes still contain a significant excess of $TFSI^-$ (0.2 M), total concentrations of the additional anion are referenced in the main text instead of the TFSI:anion ratio in the starting electrolyte (e.g., a concentrated 1:1 TFSI:Cl electrolyte contains 0.2 M Cl^-, resulting in a 0.5 mM Cl^- concentration in the dilute electrolyte for a total M^{2+} concentration of 0.5 mM).

Supporting Electrolyte Selection: TBATFSI (TBA = tetrabutylammonium), LiTFSI and NaTFSI were all considered as supporting electrolytes to enable electrochemical measurements with dilute concentrations of working divalent cations. Although the nature of the supporting electrolyte cation does induce some changes in reversibility of the observed electrochemistry (Figure S12), no significant changes to the overall electrochemical response are observed for all three systems (i.e., all major oxidation and reduction features are preserved regardless of supporting electrolyte chemistry). We further note that electrochemical alloying of Li with Zn or Mg is not expected at the potentials accessed in this work[42,43]. As a result, we conclude that the presence of a supporting electrolyte does not significantly impact the intrinsic electrochemical response of the divalent cations studied in this work. LiTFSI was therefore chosen due to the convenience of using a Li metal reference electrode regardless of working cation.

Electrochemical Characterization: All electrochemical measurements were performed in three electrode cells equipped with a Luggin capillary to enable iR drop correction. Typical iR drop correction values ranged from 100-500 Ω. Static CV measurements were performed in a cell with a total volume of 5 mL, whereas R(R)DE measurements were performed in a cell with a total volume of 35 mL. All measurements in Li- and Na-based supporting electrolytes utilized Li and Na metal, respectively, as reference electrode. Fresh metal was exposed by cutting with a scalpel prior

to insertion into the electrochemical cell, which yielded a highly stable and reproducible reference potential. Note that insertion of this type of reference electrode into the supporting electrolyte must be done prior to addition of the working divalent cation solutions, as the Li and Na metal potentials will spontaneously reduce all working cations explored in this work and render the reference electrode useless. In all other electrolytes studied, a Vycor-fritted non-aqueous electrode (BASi) filled with a saturated $AgNO_3$ solution in diglyme was employed. The potentials of $AgNO_3$-based reference electrodes were measured against a Li metal reference in LiTFSI-based supporting electrolyte in order to enable consistent referencing to the Li/Li^+ potential. Measurements in Na-based electrolytes with Na metal references were re-referenced to Li/Li^+ using the standard Na/Na^+ potential. As a result, all potentials are reported vs. Li/Li^+. Mg, Zn and Cu counter electrodes (≥ 99.9985% purity) were used as appropriate for the specific working cation under investigation.

Electrochemical measurements were performed using an Autolab potentiostat equipped with a bipotentiostat in order to enable RRDE measurements. R(R)DE measurements employed a Pine rotator to control rotation rate during electrochemical measurements. In all cases, 6 mm diameter glassy carbon disks were used as the working electrode, and were assembled using a Teflon u-cap and Kel-F collet. RRDE measurements employed a similar setup utilizing a Kel-F collet containing an embedded Pt ring electrode. RRDE experiments involving constant metal deposition on the ring electrode utilized a hold at oxidizing potentials after every voltammogram to fully dissolve all deposited metal on the ring before measuring the next voltammogram.

Density Functional Theory:

All DFT calculations are carried out using Gaussian 16 software[44] at the ωb97xD/6-31+G(d,p)[45] level of theory using conductor-like polarizable continuum CPCM) model[46,47] employing tetrahydrofuran (THF) as the solvent medium. The initial charge of the molecular complex is determined based on the most stable oxidation state of the metal cation (i.e. +2 for Mg and Zn) and the number of anions (with oxidation state of -1) present in the complex. The initial geometries of the complexes are optimized in the initial charge state and after 1 e^- and 2 e^- reductions. In the case of 2 e^- reduction, molecular complexes are optimized in both singlet and triplet spin states. The 1 e^- ($E^{red,1}$ w.r.t. Li/Li^+) and 2 e^- ($E^{red,2}$ w.r.t. Li/Li^+) reduction potentials of the complexes are calculated using the change in Gibbs free energy in solution medium at 298 K upon addition of 1 e^- and 2 e^- to the initial complexes using equation 1:

$$E^{red} = \frac{-\triangle G^{red}}{nF} - 1.24\ \text{V} \quad (1)$$

Here F is the Faraday constant (eV) and n is the number of electrons added to the initial complex (n = 1, 2 for 1 e^- and 2 e^- reductions, respectively). The constant value of 1.24 V is subtracted to convert the change in Gibbs free energy to the reduction potential (Li/Li^+ reference electrode). More details about the calculation of redox potential can be found elsewhere[48–53]. The binding enthalpies of different anions (Cl^-, OTf^-, $TFSI^-$, BF_4^- and PF_6^-) with the divalent metal cations (Mg^{2+} and Zn^{2+}) are calculated using equation 2.

$$\triangle H = H_{complex} - (H_{M^{2+}(DG)} + n*H_{anion}) \quad (2)$$

Here $H_{complex}$, $H_{M^{2+}(DG)}$ and H_{anion} are the computed enthalpies of the complex, divalent metal ion-1 diglyme complex and anion molecule at 298 K, respectively. The 'n' is the total number of anions in the complex (n = 1,2 for mono and di-anion complexes).

Supporting Information

Additional electrochemical measurements and results of DFT calculations summarizing reduction potentials and binding energies of multiple Zn^{2+} and Mg^{2+} complexes with diglyme, Cl^-, $TFSI^-$, OTf^-, BF_4^- and PF_6^-.

Acknowledgements

This work was supported as part of the Joint Center for Energy Storage Research (JCESR), an Energy Innovation Hub funded by the U.S. Department of Energy, Office of Science, Basic Energy Sciences. Electrochemical measurements were performed at the Electrochemical Discovery Laboratory, a JCESR facility at Argonne National Laboratory. We acknowledge a generous grant of computer time from the Argonne National Laboratory Computing Resource Center (Bebop). We also acknowledge the computational resources from Center for Nanoscale Materials, an Office of Science user facility, which was supported by the U.S. Department of Energy, Office of Science, Office of Basic Energy Sciences under Contract no. DE-AC02-06CH11357.

References

(1) Crabtree, G.; Kócs, E.; Trahey, L. The Energy-Storage Frontier: Lithium-Ion Batteries and Beyond. *MRS Bull.* **2015**, *40*, 1067–1078.

(2) Canepa, P.; Sai Gautam, G.; Hannah, D. C.; Malik, R.; Liu, M.; Gallagher, K. G.; Persson, K. A.; Ceder, G. Odyssey of Multivalent Cathode Materials: Open Questions and Future Challenges. *Chem. Rev.* **2017**, *117*, 4287–4341.

(3) Li, M.; Lu, J.; Ji, X.; Li, Y.; Shao, Y.; Chen, Z.; Zhong, C.; Amine, K. Design Strategies for Nonaqueous Multivalent-Ion and Monovalent-Ion Battery Anodes. *Nat. Rev. Mater.* **2020**, *5*, 276–294.

(4) Aurbach, D.; Lu, Z.; Schechter, A.; Gofer, Y.; Gizbar, H.; Turgeman, R.; Cohen, Y.; Moshkovich, M.; Levi, E. Prototype Systems for Rechargeable Magnesium Batteries. *Nature* **2000**, *407*, 724–727.

(5) Tepavcevic, S.; Liu, Y.; Zhou, D.; Lai, B.; Maser, J.; Zuo, X.; Chan, H.; Král, P.; Johnson, C. S.; Stamenkovic, V.; Markovic, N. M.; Rajh, T. Nanostructured Layered Cathode for Rechargeable Mg-Ion Batteries. *ACS Nano* **2015**, *9*, 8194–8205.

(6) Kim, C.; Phillips, P. J.; Key, B.; Yi, T.; Nordlund, D.; Yu, Y.-S.; Bayliss, R. D.; Han, S.-D.; He, M.; Zhang, Z.; Burrell, A. K.; Klie, R. F.; Cabana, J. Direct Observation of Reversible Magnesium Ion Intercalation into a Spinel Oxide Host. *Adv. Mater.* **2015**, *27*, 3377–3384.
(7) Nazar, L.; Sun, X.; Duffort, V.; Bonnick, P.; Rong, Z.; Liu, M.; Persson, K.; Ceder, G. A High Capacity Thiospinel Cathode for Mg Batteries. *Energy Environ. Sci.* **2016**, *9*, 2273–2277.
(8) Sun, X.; Duffort, V.; Mehdi, B. L.; Browning, N. D.; Nazar, L. F. Investigation of the Mechanism of Mg Insertion in Birnessite in Nonaqueous and Aqueous Rechargeable Mg-Ion Batteries. *Chem. Mater.* **2016**, *28*, 534–532.
(9) Sun, X.; Blanc, L.; Nolis, G. M.; Bonnick, P.; Cabana, J.; Nazar, L. F. NaV1.25Ti0.75O4: A Potential Post-Spinel Cathode Material for Mg Batteries. *Chem. Mater.* **2018**, *30*, 121–128.
(10) Yoo, H. D.; Jokisaari, J. R.; Yu, Y.-S.; Kwon, B. J.; Hu, L.; Kim, S.; Han, S.-D.; Lopez, M.; Lapidus, S. H.; Nolis, G. M.; Ingram, B. J.; Bolotin, I.; Ahmed, S.; Klie, R. F.; Vaughey, J. T.; Fister, T. T.; Cabana, J. Intercalation of Magnesium into a Layered Vanadium Oxide with High Capacity. *ACS Energy Lett.* **2019**, *4*, 1528–1534.
(11) Bayliss, R. D.; Key, B.; Sai Gautam, G.; Canepa, P.; Kwon, B. J.; Lapidus, S. H.; Dogan, F.; Adil, A. A.; Lipton, A. S.; Baker, P. J.; Ceder, G.; Vaughey, J. T.; Cabana, J. Probing Mg Migration in Spinel Oxides. *Chem. Mater.* **2019**, *32*, 663–670.
(12) Kwon, B. J.; Lau, K.-C.; Park, H.; Wu, Y. A.; Hawthorne, K. L.; Li, H.; Kim, S.; Bolotin, I. L.; Fister, T. T.; Zapol, P.; Klie, R. F.; Cabana, J.; Liao, C.; Lapidus, S. H.; Key, B.; Vaughey, J. T. Probing Electrochemical Mg-Ion Activity in MgCr2–XVxO4 Spinel Oxides. *Chem. Mater.* **2020**, *32*, 1162–1171.
(13) Gregory, T. D.; Hoffman, R. J.; Winterton, R. C. Nonaqueous Electrochemistry of Magnesium Applications to Energy Storage. *J. Electrochem. Soc.* **1990**, *137*, 775–780.
(14) Liebenow, C.; Yang, Z.; Lobitz, P. The Electrodeposition of Magnesium Using Solutions of Organomagnesium Halides, Amidomagnesium Halides and Magnesium Organoborates. *Electrochem. Commun.* **2000**, *2*, 641–645.
(15) Mizrahi, O.; Amir, N.; Pollak, E.; Chusid, O.; Marks, V.; Gottlieb, H.; Larush, L.; Zinigrad, E.; Aurbach, D. Electrolyte Solutions with a Wide Electrochemical Window for Rechargeable Magnesium Batteries. *J. Electrochem. Soc.* **2008**, *155*, A103–A109.
(16) NuLi, Y.; Yang, J.; Wang, J.; Xu, J.; Wang, P. Electrochemical Magnesium Deposition and Dissolution with High Efficiency in Ionic Liquid. *Electrochem. Solid-State Lett.* **2005**, *8*, C166–C169.
(17) Tutusaus, O.; Mohtadi, R.; Arthur, T. S.; Mizuno, F.; Nelson, E. G.; Sevryugina, Y. V. An Efficient Halogen-Free Electrolyte for Use in Rechargeable Magnesium Batteries. *Angew. Chem. Int. Ed.* **2015**, *54*, 7900–7904.
(18) Keyzer, E. N.; Glass, H. F. J.; Liu, Z.; Bayley, P. M.; Dutton, S. E.; Grey, C. P.; Wright, D. S. Mg(PF6)2-Based Electrolyte Systems: Understanding Electrolyte–Electrode Interactions for the Development of Mg-Ion Batteries. *J. Am. Chem. Soc.* **2016**, *138*, 8682–8685.
(19) Hahn, N. T.; Seguin, T. J.; Lau, K.-C.; Liao, C.; Ingram, B. J.; Persson, K. A.; Zavadil, K. R. Enhanced Stability of the Carba-Closo-Dodecaborate Anion for High-Voltage Battery Electrolytes through Rational Design. *J. Am. Chem. Soc.* **2018**, *140*, 11076–11084.

(20) Zhao-Karger, Z.; Bardaji, E. G.; Fuhr, O.; Fichtner, M. New Class of Non-Corrosive, Highly Efficient Electrolytes for Rechargeable Magnesium Batteries. *J. Mater. Chem. A* **2017**, *5*, 10815–10820.
(21) Lau, K.-C.; Seguin, T. J.; Carino, E. V.; Hahn, N. T.; Connell, J. G.; Ingram, B. J.; Persson, K. A.; Zavadil, K. R.; Liao, C. Widening Electrochemical Window of Mg Salt by Weakly Coordinating Perfluoroalkoxyaluminate Anion for Mg Battery Electrolyte. *J. Electrochem. Soc.* **2019**, *166*, A1510–A1519.
(22) Nam, K. W.; Kim, S.; Lee, S.; Salama, M.; Shterenberg, I.; Gofer, Y.; Kim, J.-S.; Yang, E.; Park, C. S.; Kim, J.-S.; Lee, S.-S.; Chang, W.-S.; Doo, S.-G.; Jo, Y. N.; Jung, Y.; Aurbach, D.; Choi, J. W. The High Performance of Crystal Water Containing Manganese Birnessite Cathodes for Magnesium Batteries. *Nano Lett.* **2015**, *15*, 4071–4079.
(23) Lipson, A. L.; Han, S.-D.; Kim, S.; Pan, B.; Sa, N.; Liao, C.; Fister, T. T.; Burrell, A. K.; Vaughey, J. T.; Ingram, B. J. Nickel Hexacyanoferrate, a Versatile Intercalation Host for Divalent Ions from Nonaqueous Electrolytes. *J. Power Sources* **2016**, *325*, 646–652.
(24) Lipson, A. L.; Han, S.-D.; Pan, B.; See, K. A.; Gewirth, A. A.; Liao, C.; Vaughey, J. T.; Ingram, B. J. Practical Stability Limits of Magnesium Electrolytes. *J. Electrochem. Soc.* **2016**, *163*, A2253.
(25) Song, J.; Sahadeo, E.; Noked, M.; Lee, S. B. Mapping the Challenges of Magnesium Battery. *J. Phys. Chem. Lett.* **2016**, *7*, 1736–1749.
(26) Muldoon, J.; Bucur, C. B.; Gregory, T. Fervent Hype behind Magnesium Batteries: An Open Call to Synthetic Chemists - Electrolytes and Cathodes Needed. *Angew. Chem.* **2017**, *56*, 12064–12084.
(27) Doe, R. E.; Han, R.; Hwang, J.; Gmitter, A. J.; Shterenberg, I.; Yoo, H. D.; Pour, N.; Aurbach, D. Novel, Electrolyte Solutions Comprising Fully Inorganic Salts with High Anodic Stability for Rechargeable Magnesium Batteries. *Chem. Commun.* **2014**, *50*, 243–245.
(28) Shterenberg, I.; Salama, M.; Yoo, H. D.; Gofer, Y.; Park, J.-B.; Sun, Y.-K.; Aurbach, D. Evaluation of (CF3SO2)2N- (TFSI) Based Electrolyte Solutions for Mg Batteries. *J. Electrochem. Soc.* **2015**, *162*, A7118–A7128.
(29) He, Y.; Li, Q.; Yang, L.; Yang, C.; Xu, D. Electrochemical-Conditioning-Free and Water-Resistant Hybrid AlCl3/MgCl2/Mg(TFSI)2 Electrolytes for Rechargeable Magnesium Batteries. *Angew. Chem. Int. Ed.* **2019**, *58*, 7615–7619.
(30) Connell, J. G.; Genorio, B.; Lopes, P. P.; Strmcnik, D.; Stamenkovic, V. R.; Markovic, N. M. Tuning the Reversibility of Mg Anodes via Controlled Surface Passivation by H2O/Cl– in Organic Electrolytes. *Chem. Mater.* **2016**, *28*, 8268–8277.
(31) Ta, K.; See, K. A.; Gewirth, A. A. Elucidating Zn and Mg Electrodeposition Mechanisms in Nonaqueous Electrolytes for Next-Generation Metal Batteries. *J. Phys. Chem. C* **2018**, *122*, 13790–13796.
(32) Nekrasov, L.; Besezina, N. Use Of A Disc Electrode With A Ring In Studying Electrolytic Reduction Of Copper. *Dokl. Akad. Nauk SSSR* **1962**, *142*, 855–858.
(33) Markovic, N.; Ross, P. N. Effect of Anions on the Underpotential Deposition of Copper on Platinum(111) and Platinum(100) Surfaces. *Langmuir* **1993**, *9*, 580–590.
(34) Markovic, N. M.; Gasteiger, H. A.; Ross, P. N. Jr. Copper Electrodeposition on Pt(111) in the Presence of Chloride and (Bi)Sulfate: Rotating Ring-Pt(111) Disk Electrode Studies. *Langmuir* **1995**, *11*, 4098–4108.

(35) Opekar, F.; Beran, P. Rotating Disk Electrodes. *J. Electroanal. Chem. Interfacial Electrochem.* **1976**, *69*, 1–105.
(36) Rajput, N. N.; Qu, X.; Sa, N.; Burrell, A. K.; Persson, K. A. The Coupling between Stability and Ion Pair Formation in Magnesium Electrolytes from First-Principles Quantum Mechanics and Classical Molecular Dynamics. *J. Am. Chem. Soc.* **2015**, *137*, 3411–3420.
(37) Baskin, A.; Prendergast, D. Exploration of the Detailed Conditions for Reductive Stability of $Mg(TFSI)_2$ in Diglyme: Implications for Multivalent Electrolytes. *J. Phys. Chem. C* **2016**, *120*, 3583–3594.
(38) Yu, Y.; Baskin, A.; Valero-Vidal, C.; Hahn, N. T.; Liu, Q.; Zavadil, K. R.; Eichhorn, B. W.; Prendergast, D.; Crumlin, E. J. Instability at the Electrode/Electrolyte Interface Induced by Hard Cation Chelation and Nucleophilic Attack. *Chem. Mater.* **2017**, *29*, 8504–8512.
(39) Han, S.-D.; Rajput, N. N.; Qu, X.; Pan, B.; He, M.; Ferrandon, M. S.; Liao, C.; Persson, K. A.; Burrell, A. K. Origin of Electrochemical, Structural, and Transport Properties in Nonaqueous Zinc Electrolytes. *ACS Appl. Mater. Interfaces* **2016**, *8*, 3021–3031.
(40) Kimura, T.; Fujii, K.; Sato, Y.; Morita, M.; Yoshimoto, N. Solvation of Magnesium Ion in Triglyme-Based Electrolyte Solutions. *J. Phys. Chem. C* **2015**, *119*, 18911–18917.
(41) Salama, M.; Shterenberg, I.; Gizbar, H.; Eliaz, N. N.; Kosa, M.; Keinan-Adamsky, K.; Afri, M.; Shimon, L. J. W.; Gottlieb, H. E.; Major, D. T.; Gofer, Y.; Aurbach, D. Unique Behavior of Dimethoxyethane (DME)/Mg(N(SO2CF3)2)2 Solutions. *J. Phys. Chem. C* **2016**, *120*, 19586–19594.
(42) Shi, Z.; Liu, M.; Gole, J. L. Electrochemical Properties of Li - Zn Alloy Electrodes Prepared by Kinetically Controlled Vapor Deposition for Lithium Batteries. *Electrochem. Solid State Lett.* **2000**, *3*, 312.
(43) Shi, Z.; Liu, M.; Naik, D.; Gole, J. L. Electrochemical Properties of Li–Mg Alloy Electrodes for Lithium Batteries. *J. Power Sources* **2001**, *92*, 70–80.
(44) Frisch, M. J.; Trucks, G. W.; Schlegel, H. B.; Scuseria, G. E.; Robb, M. A.; Cheeseman, J. R.; Scalmani, G.; Barone, V.; Petersson, G. A.; Nakatsuji, H.; Li, X.; Caricato, M.; Marenich, A. V.; Bloino, J.; Janesko, B. G.; Gomperts, R.; Mennucci, B.; Hratchian, H. P.; Ortiz, J. V.; Izmaylov, A. F.; Sonnenberg, J. L.; Williams; Ding, F.; Lipparini, F.; Egidi, F.; Goings, J.; Peng, B.; Petrone, A.; Henderson, T.; Ranasinghe, D.; Zakrzewski, V. G.; Gao, J.; Rega, N.; Zheng, G.; Liang, W.; Hada, M.; Ehara, M.; Toyota, K.; Fukuda, R.; Hasegawa, J.; Ishida, M.; Nakajima, T.; Honda, Y.; Kitao, O.; Nakai, H.; Vreven, T.; Throssell, K.; Montgomery Jr., J. A.; Peralta, J. E.; Ogliaro, F.; Bearpark, M. J.; Heyd, J. J.; Brothers, E. N.; Kudin, K. N.; Staroverov, V. N.; Keith, T. A.; Kobayashi, R.; Normand, J.; Raghavachari, K.; Rendell, A. P.; Burant, J. C.; Iyengar, S. S.; Tomasi, J.; Cossi, M.; Millam, J. M.; Klene, M.; Adamo, C.; Cammi, R.; Ochterski, J. W.; Martin, R. L.; Morokuma, K.; Farkas, O.; Foresman, J. B.; Fox, D. J. *Gaussian 16 Rev. C.01*; Wallingford, CT, 2016.
(45) Chai, J.-D.; Head-Gordon, M. Long-Range Corrected Hybrid Density Functionals with Damped Atom–Atom Dispersion Corrections. *Phys. Chem. Chem. Phys.* **2008**, *10*, 6615–6620.
(46) Cossi, M.; Rega, N.; Scalmani, G.; Barone, V. Energies, Structures, and Electronic Properties of Molecules in Solution with the C-PCM Solvation Model. *J. Comput. Chem.* **2003**, *24*, 669–681.

(47) Barone, V.; Cossi, M. Quantum Calculation of Molecular Energies and Energy Gradients in Solution by a Conductor Solvent Model. *J. Phys. Chem. A* **1998**, *102*, 1995–2001.
(48) Guerard, J. J.; Arey, J. S. Critical Evaluation of Implicit Solvent Models for Predicting Aqueous Oxidation Potentials of Neutral Organic Compounds. *J. Chem. Theory Comput.* **2013**, *9*, 5046–5058.
(49) Moens, J.; Geerlings, P.; Roos, G. A Conceptual DFT Approach for the Evaluation and Interpretation of Redox Potentials. *Chem. – Eur. J.* **2007**, *13*, 8174–8184.
(50) Borodin, O.; Behl, W.; Jow, T. R. Oxidative Stability and Initial Decomposition Reactions of Carbonate, Sulfone, and Alkyl Phosphate-Based Electrolytes. *J. Phys. Chem. C* **2013**, *117*, 8661–8682.
(51) Phillips, K. L.; Sandler, S. I.; Chiu, P. C. A Method to Calculate the One-Electron Reduction Potentials for Nitroaromatic Compounds Based on Gas-Phase Quantum Mechanics. *J. Comput. Chem.* **2011**, *32*, 226–239.
(52) Vollmer, J. M.; Curtiss, L. A.; Vissers, D. R.; Amine, K. Reduction Mechanisms of Ethylene, Propylene, and Vinylethylene Carbonates: A Quantum Chemical Study. *J. Electrochem. Soc.* **2003**, *151*, A178.
(53) Kelly, C. P.; Cramer, C. J.; Truhlar, D. G. Single-Ion Solvation Free Energies and the Normal Hydrogen Electrode Potential in Methanol, Acetonitrile, and Dimethyl Sulfoxide. *J. Phys. Chem. B* **2007**, *111*, 408–422.